

Experimental study on dynamic fracture behavior of AISI 5140 steel over a wide range of loading rates

Qiaoguo Wu¹, Defu Nie², Jianhua Pan¹, changzheng cheng¹, and Xuan Wang¹

¹Hefei University of Technology

²National Safety Engineering Technology Research Center for Pressure Vessels and Pipelines

June 22, 2020

Abstract

Experimental studies were conducted on the dynamic fracture behavior of AISI 5140 steel over a wide range of loading rates. True stress-strain relations of the steel were measured under different strain rates, and a dynamic constitutive model was then expressed with the strain-hardening term and the strain-rate hardening term. Fracture tests were investigated under quasi-static condition, instrumented Charpy impact condition and Hopkinson pressure bar impact condition. Fracture toughnesses corresponding to each test condition were also determined. Fracture characteristics were analyzed with observations of the fracture appearances. It was found that the fracture toughness decreased significantly with the increasing loading rate, and the fracture mechanisms of the steel at various loading rates were brittle fractures characterized by river markings and secondary cracks. Based on the fracture assessment method of the CEGB R6 procedure, the effects of the strain rate and the loading rate on the assessment curve were discussed.

1 — INTRODUCTION

The evaluation of the dynamic fracture behavior of engineering materials has an important significance for the assurance of the integrity and safety of structural components subjected to various dynamic loads, such as impact, explosion, or earthquake. Since the loading rate range of these dynamic loads is very wide, a more comprehensive understanding of the relationship between the fracture behavior and the loading rate is necessary.^{1,2}

Some research has been carried out on the area of dynamic fracture. For the complexity of the dynamic fracture process, theoretical methods are limited and tests are the main means of dynamic fracture mechanics research. Three ranges are divided according to the loading rate \dot{K}_I : low loading rate range ($10^{-3} \text{ MPa} \frac{\sqrt{m}}{s} \leq \dot{K}_I < 10^3 \text{ MPa} \frac{\sqrt{m}}{s}$), at which it is regarded as quasi-static loading and belongs to quasi-static fracture; medium loading rate range ($10^3 \text{ MPa} \frac{\sqrt{m}}{s} \leq \dot{K}_I < 10^5 \text{ MPa} \frac{\sqrt{m}}{s}$), at which the influence of inertia effect should be considered; and high loading rate range ($\dot{K}_I \geq 10^5 \text{ MPa} \frac{\sqrt{m}}{s}$), at which it must consider the interaction between stress wave and crack in addition to the influence of inertia effect. According to different loading rates, different types of loading test devices can be selected. The experimental techniques for dynamic fracture often include the drop-weight impact test, instrumented Charpy impact test, and Hopkinson pressure bar (HPB) impact test.³⁻⁶

Chaouadi and Puzzolante⁷ examined the dynamic fracture toughness of ferritic steel with an instrumented Charpy impact test. The dynamic fracture toughness was greater than the quasi-static one. Similar conclusions were obtained in Foster et al.⁸ and Prasad et al.⁹, where fracture toughness of the 4340 steel and Al-Li

8090 alloy increased with the increasing loading rate. Wu et al.¹⁰ performed experimental studies on the dynamic fracture behavior of FV520B steel under quasi-static and dynamic loading conditions, and the fracture toughness increased linearly with the increasing loading rate. Galvez et al.¹¹ conducted experimental studies on the fracture behavior of high strength steel ArmoX500T, and the static and dynamic fracture toughnesses were quite similar. The fracture toughness without a marked loading rate effect was also determined for Al 7075-T651.¹² Different from these insensitive ones, the irregular relation of the fracture toughness and the loading rate was observed experimentally for 685 homogeneous steel.¹³ When the loading rate was less than 1.8778 MPa.m^{0.5}, the dynamic fracture toughness decreased with the increasing loading rate. However, when the loading rate was greater than 1.8778 MPa.m^{0.5}, the dynamic fracture toughness rose due to the effect of thermal softening near the crack tip. Additionally, Wu et al.¹⁴ conducted an experimental study on fracture behavior of AISI 1045 steel. The fracture modes exhibited a transition from ductile to brittle fracture with the increasing loading rate, and the dynamic fracture toughness was less than the quasi-static one. A similar conclusion was also obtained in Lorentzon et al.¹⁵ for the ordinary C-Mn structural steel. According to the published reports, it was found that when the loading rate increased, some fracture toughnesses increased, some decreased, and other fracture toughness levels changed insensitively or irregularly.

AISI 5140 steel, also named 40Cr steel, has been widely used in engineering structures, and investigations on the dynamic fracture behaviors are related to many engineering problems. Xu and Li¹⁶ carried out the fracture test of 40Cr steel loaded by HPB and the fracture toughness of the steel increased with the increasing loading rate. However, for the same material, a conflicting result was obtained in Li et al.¹⁷, where the fracture toughness decreased with the increasing loading rate. It should be noted that in Refs. 16 and 17, the fracture toughnesses were both determined by the numerical-experimental method, but the dynamic constitutive relation of the steel was not considered in the numerical simulations. Besides, as described in the literature, the loading rate range tested may not be wide enough, resulting in inconsistent conclusions. Few results can be found on the fracture toughness and fracture mechanism of the steel over a wide range of loading rates.

In this paper, experimental studies were performed on the fracture behavior of AISI 5140 steel over a wide range of loading rates. True stress-strain relations were measured and the dynamic constitutive model was proposed. Fracture tests under quasi-static condition, instrumented Charpy impact condition, and HPB impact condition were carried out, and fracture toughnesses and characteristics were analyzed. Comparisons and discussions of the fracture behaviors under the above loading rates were conducted in terms of fracture modes and fracture toughness values. Finally, based on the fracture assessment method of the CEBG R6 procedure, the effects of the strain rate and the loading rate on the assessment curve were discussed.

2 — TEST MATERIAL AND CONSTITUTIVE RELATION

The AISI 5140 steel was obtained from a large reciprocating compressor crankshaft with a diameter of 200 mm. The crankshaft was first forged with a temperature between 850 and 1150 °C and air cooled to room temperature. Then it underwent the heat treatment process with a quenching temperature 850 of°C, a tempering temperature of 590°C and cooling with oil. The chemical compositions of the steel were measured and are listed in Table 1. The microstructure of the AISI 5140 steel was mainly composed of fine pearlites, tempered sorbites and proeutectoid ferrites around prior austenite grain boundaries, and the grain size was about 20-30 μm, as shown in Figure 1.

Quasi-static and dynamic mechanical properties of the AISI 5140 steel were measured using the electro-hydraulic servo testing machine and HPB. True stress-strain curves in the plastic stage are presented in Figure 2, and yield strengths of the steel at different strain rates are shown in Figure 3. The dynamic yield strengths are 847.7 MPa and 892.0 MPa at the strain rates 3057 s⁻¹ and 4700 s⁻¹ respectively, which increased by 37.8% and 45.0% compared to the quasi-static value 615.2 MPa. The dynamic yield strength σ_{yd} can be expressed with the quasi-static one σ_{ys} and the strain rate $\dot{\epsilon}$ in Cowper-Symons form:

$$\sigma_{yd} = \sigma_{ys} \left(1 + \frac{\dot{\epsilon}_{eq}}{C} \right)^{\frac{1}{p}} \quad (1)$$

where $C = 257.8$, and $p = 8.0$ are material constants related to strain-rate hardening.

As shown in Figure 2, the AISI 5140 steel is sensitive to strain rate and the flow stress increases with the increasing strain. Therefore, the dynamic constitutive relation of the steel is expressed with the strain hardening term and the strain-rate hardening term

$$\sigma_{\text{eq}} = (A_1 + A_2 \varepsilon_{\text{eq}}^n) \left(1 + \frac{\dot{\varepsilon}_{\text{eq}}}{C}\right)^{\frac{1}{p}} \quad (2)$$

where σ_{eq} is equivalent stress, ε_{eq} is equivalent strain, and $\dot{\varepsilon}_{\text{eq}}$ is equivalent strain rate. $A_1 = 615.2$ MPa, $A_2 = 863.7$ MPa, and $n = 0.45$ are material constants related to strain hardening. It is clear from Figures 2 and 3 that the test data of the stress-strain relation and the yield strength-strain rate relation can be well explained by Equations (1) and (2).

3 — FRACTURE TOUGHNESS TESTS UNDER DIFFERENT LOADING CONDITIONS

3.1 — FRACTURE TOUGHNESS UNDER QUASI-STATIC CONDITION

Quasi-static fracture tests were performed in accordance with GB/T 21143-2007¹⁸. Three-point bending specimens were adopted, and the thickness (B), width (W), length (L), span (S), and initial crack length (a_0) are 10 mm, 20 mm, 100 mm, 80 mm and 12 mm, respectively. The tests were performed with the electro-hydraulic servo fatigue testing machine. Three repetitive test results of the load-deflection curves are presented in Figure 4.

The quasi-static fracture toughness (K_{IC}) is determined by

$$K_{\text{IC}} = \left[\left(\frac{S}{W} \right) \frac{F_Q}{(B^2 W)^{0.5}} \right] g_1 \left(\frac{a_0}{W} \right) \quad (3)$$

$$g_1 \left(\frac{a_0}{W} \right) = \frac{3 \left(\frac{a_0}{W} \right)^{0.5} \left[1.99 - \left(\frac{a_0}{W} \right) \left(1 - \frac{a_0}{W} \right) \left(2.15 - \frac{3.93 a_0}{W} + \frac{2.7 a_0^2}{W^2} \right) \right]}{2 \left(1 + \frac{2 a_0}{W} \right) \left(1 - \frac{a_0}{W} \right)^{1.5}} \quad (4)$$

where F_Q is the value of the load at the intersection point of the load-deflection curve and the line (OF_d). The slope of OF_d is 0.96 times of that of the initial linear part of the load-deflection curve¹⁸. Substituting the F_Q values 5421 N, 5598 N and 5493 N into Equation (3), the fracture toughnesses (K_{IC}) of 63.4 MPa.m^{0.5}, 64.8 MPa.m^{0.5}, and 62.1 MPa.m^{0.5} are obtained for the three tests, respectively. The average fracture toughness is 63.4 MPa.m^{0.5}.

3.2 — FRACTURE TOUGHNESS UNDER INSTRUMENTED CHARPY IMPACT CONDITION

Fracture toughness tests under instrumented Charpy impact condition were conducted in accordance with GB/T 229-2007¹⁹. The single edge-through cracked Charpy impact specimens were utilized with the thickness (B), width (W), length (L), span (S), and initial crack length (a_0) of 10 mm, 10 mm, 55 mm, 40 mm and 6 mm, respectively.

Three repetitive test results of the load-deflection curves are presented in Figure 5. For the load-deflection curve without yield stage, the crack initiation time (t_f) was determined as the time at which the load reached the peak value (P_{max}) and the dynamic fracture toughness could be determined by linear elastic fracture mechanics²⁰

$$K_{\text{Id}} = \frac{P_{\text{max}} S}{B W^{1.5}} f \left(\frac{a_0}{W} \right) \quad (5)$$

$$f \left(\frac{a_0}{W} \right) = \frac{3 \left(\frac{a_0}{W} \right)^{0.5} \times \left[1.99 - \left(\frac{a_0}{W} \right) \times \left(1 - \frac{a_0}{W} \right) \right] \times \left(2.15 - 3.93 \frac{a_0}{W} + 2.7 \frac{a_0^2}{W^2} \right)}{2 \times \left(1 + 2 \frac{a_0}{W} \right) \times \left(1 - \frac{a_0}{W} \right)^{1.5}} \quad (6)$$

The peak loads are 3.16 kN, 3.29 kN and 3.27 kN, with the corresponding t_f being 0.128 ms, 0.116 ms and 0.120 ms, respectively. According to Equation (5), the dynamic fracture toughnesses are 47.7 MPa.m^{0.5}, 49.6 MPa.m^{0.5}, 49.3 MPa.m^{0.5}, and the loading rates ($\dot{K}_{\text{Id}} = K_{\text{Id}}/t_f$) are 3.72×10^5 MPa.m^{0.5}/s, 3.88×10^5

MPa.m^{0.5}/s and 3.74×10⁵ MPa.m^{0.5}/s, respectively. The average dynamic fracture toughness and loading rate are 48.9 MPa.m^{0.5} and 3.78×10⁵MPa.m^{0.5}/s, respectively.

3.3 — FRACTURE TOUGHNESS UNDER HPB IMPACT CONDITION

3.3.1 — FRACTURE TEST

The principle of the dynamic fracture test system loaded by HPB can be referred to Ref. 12. The projectile and the incident bar are both cylindrical and 14.5 mm in diameter, and 300 mm and 1000 mm in length. The incident bar end in contact with the specimen exhibits a wedge shape with a wedge angle of 60° and a fillet radius of 2 mm. The specimens utilized in the HPB impact test were the same as the quasi-static test. The crack initiation time was evaluated by a small strain gauge mounted on the specimen.

Figure 6 shows the incident and reflected strain waves, and Figure 7 shows the crack initiation signals of the specimens. The crack initiation time (t_f) can be derived from the crack initiation signal

$$t_f = t_p - t_d \quad (7)$$

where t_p is the time corresponding to the peak strain signal and t_d is the propagating time of the strain wave from the crack tip to the position of the strain gauge. Three repetitive tests were conducted and the average crack initiation time was calculated to be 31 us according to Equation (7).

The displacement of the incident bar end initially in contact with the specimen $D(t)$ was calculated from one-dimensional elastic wave propagation theory

$$D(t) = \int_0^t c [\varepsilon_i(t) - \varepsilon_r(t)] dt \quad (8)$$

where $\varepsilon_i(t)$ and $\varepsilon_r(t)$ are incident and reflected strains, c is the sound speed in the incident bar ($c = \sqrt{\frac{E}{\rho}}$), and ρ is the density of the incident bar. For the steel bar used in the test, the density (ρ) is taken to be 7800 kg/m³. Since the test data of the three specimens were consistent (see Figures 6 and 7), the data of specimen-1 was selected to be analyzed in the following. Figure 8 shows the displacement of the incident bar end initially in contact with the specimen.

3.3.2 — DETERMINATION OF FRACTURE TOUGHNESS

A numerical-experimental method was adopted to determine the fracture toughness. The finite element model was established with ABAQUS based on the test parameters. Only one quarter of the incident bar and the specimen, as well as half of one roller support, was modeled because of the geometric symmetry, as shown in Figure 9. For simplification, the incident stress wave calculated from the experimental strain wave was used as the input load exerted to the free end of the incident bar¹⁶. The C3D8R elements were used for the whole model. The incident bar model was meshed with 9137 nodes and 6128 elements, and the support model was meshed with 486 nodes and 336 elements. The specimen model was first meshed with 6660 nodes and 5220 elements, and the mesh of the crack tip and adjacent area were then refined (see Figure 9). The face-to-face contact algorithm was assigned in the model.

A linear elastic constitutive relation was adopted for the incident bar and the support. The elastic modulus, the Poisson ratio and the density were taken to be 210 GPa, 0.3 and 7800 kg/m³, respectively. For the AISI 5140 steel, the dynamic constitutive relation considering strain hardening and strain-rate hardening (see Equation (2)) was utilized. The constitutive relation was implemented by utilizing a user-defined subroutine UMAT.

Since the specimen exhibited a brittle fracture characteristic that satisfied the small-scale yield condition, the stress intensity factor (K_I) can be calculated from J -integral²¹

$$K_I = \sqrt{\frac{EJ}{(1-\nu^2)}} \quad (9)$$

where E is the elastic modulus and ν is Poisson's ratio.

Numerical strain history at the strain gauge position of the specimen is shown in Figure 7 and agrees well with the tests before the crack initiation time of 31 us. After this time, the numerical strain kept increasing while the test strain decreased. The reason for this difference is because the fracture process is not considered in the simulation. Figure 8 shows a comparison of the numerical and experimental displacement histories of the bar end initially in contact with the specimen. The numerical result also agrees well with the test data before the crack initiation time, and begins to deviate from the test after this time since the specimen actually fractures. It is clear from Figures 7 and 8 that the simulation is reliable until the crack initiates.

The numerical J -integral history at the crack tip is shown in Figure 10. The fracture toughness (J_{Id}) is 6.85 MPa.mm according to $t_f = 31$ us. From Equation (9), the fracture toughness ($K_{Id} = 38.8 \text{ MPa.m}^{0.5}$) and the loading rate ($\dot{K}_{Id} = 1.25 \times 10^6 \text{ MPa.m}^{0.5}/\text{s}$) are obtained.

4 — FRACTURE BEHAVIOR AND FAILURE ASSESSMENT

4.1 — FRACTURE BEHAVIOR UNDER DIFFERENT LOADING RATES

Macro and micro fracture appearances of the steel tested under different loading rates are shown in Figure 11. The fracture appearances under the three loading conditions mentioned above are similar. Brittle fracture characteristics are exhibited for the material. Macro plastic deformation near the crack tip and the lateral expansion of the specimens are not clearly observed. Brittle fracture modes with river markings and secondary cracks are also revealed from the micro appearance observations of the fractured specimens.

The fracture toughnesses of the steel under different loading rates are presented in Figure 12. The fracture toughness decreases with the increasing loading rate. Compared with the quasi-static one, the fracture toughnesses at $\dot{K}_{Id} = 3.78 \times 10^5 \text{ MPa.m}^{0.5}/\text{s}$ (under instrumented Charpy impact test) and $\dot{K}_{Id} = 1.25 \times 10^6 \text{ MPa.m}^{0.5}/\text{s}$ (under HPB impact test) decrease by 22.9% and 38.8%, respectively. The relationship of K_{Id} and \dot{K}_{Id} is described as

$$K_{Id} = K_{Id}^r - K_1 \cdot \left(\frac{\dot{K}_{Id}}{\dot{K}_{Id}^r} \right)^{c_1} \quad (10)$$

where \dot{K}_{Id}^r and K_{Id}^r are respectively the reference loading rate and reference fracture toughness value ($\dot{K}_{Id}^r = 1$, $K_{Id}^r = K_{IC} = 63.4 \text{ MPa.m}^{0.5}$), and K_1 and c_1 are experimental constants. By fitting the experimental data, K_1 and c_1 are taken to be $0.0499 \text{ MPa.m}^{0.5}$ and 0.4417 , respectively.

4.2 — DISCUSSION OF FRACTURE ASSESSMENT CURVE

The failure assessment of the cracked structure is often implemented based on the failure assessment curve (FAC) of the CEGB R6 procedure which considers both the brittle fracture failure and the plastic collapse²². However, the method is mainly utilized in static loading condition. To generalize the method to the dynamic loading conditions, the effects of the strain rate and the loading rate are introduced into the FAC equation and discussed.

The FAC curve equation based on option 1 in the CEGB R6 procedure is expressed in the following form²²

$$K_{rd} = \begin{cases} (1 + 0.5L_{rd}^2)^{-0.5} (0.3 + 0.7e^{-0.6 L_{rd}^6}) & L_{rd} \leq L_{rd}^{\max} \\ 0 & L_{rd} > L_{rd}^{\max} \end{cases} \quad (11)$$

where K_{rd} is the ratio of stress intensity factor at the crack tip to the dynamic fracture toughness of material ($K_{rd} = \frac{K_I}{K_{Id}}$), L_{rd} is defined as the ratio of the loading condition assessed for the plastic limit load of the structure ($L_{rd} = \frac{\sigma_{ref}}{\sigma_{yd}}$), σ_{ref} is the reference stress, L_{rd}^{\max} is the cut-off value of the L_{rd} and is taken to be 1.20 here. Corresponding to the static value $K_r = \frac{K_I}{K_{IC}}$, $L_r = \frac{\sigma_{ref}}{\sigma_{ys}}$ and according to the relationship of dynamic fracture toughness and loading rate, as well as the relationship of dynamic yield strength and strain rate, the dynamic FAC equation can be expressed as

$$K_r = \begin{cases}$$

$$f_2(\dot{K}_I) \left[1 + 0.5 \left(\frac{L_r}{f_1(\dot{\epsilon})} \right)^2 \right]^{-0.5} \left[0.3 + 0.7e^{-0.6 \left(\frac{L_r}{f_1(\dot{\epsilon})} \right)} L_{rd}^6 \right] \quad \begin{array}{l} L_r \leq L_r^{\max} \\ L_r > L_r^{\max} \end{array} \quad (12)$$

where $f_1(\dot{\epsilon}) = \frac{\sigma_{vd}}{\sigma_{ys}} = \left(1 + \frac{\dot{\epsilon}_{eq}}{C} \right)^{\frac{1}{p}}$, $f_2(\dot{K}_I) = \frac{K_{Id}}{K_{IC}} = 1 - \frac{K_1}{K_{IC}} \left(\frac{\dot{K}_{Id}}{K_{Id}^*} \right)^{c_1}$.

The effects of the loading rate and the strain rate on failure assessment curves are discussed. Figure 13 shows the dynamic failure assessment diagram (FAD) of the AISI 5140 steel under different loading rates and strain rates. Figure 13(A) shows the relationship between the FAC and the loading rate. The black curve is the static FAC, and the red and blue curves are dynamic FAC at the loading rates of $\dot{K}_I=5 \times 10^5$ MPa.m^{0.5}/s and $\dot{K}_I=1 \times 10^6$ MPa.m^{0.5}/s with the same strain rate $\dot{\epsilon}=1 \times 10^2$ s⁻¹. The structure is acceptable if the assessment point (L_r , K_r) of a cracked structure is on or inside the FAD. Otherwise, the structure is unacceptable. It is clear from Figure 13(A) that the acceptable zone decreases with an increase in the loading rate. Figure 13(B) shows the relationship between the FAC and the strain rate. The black curve is static FAC, and the red and the blue curves are dynamic FAC at the strain rates of $\dot{\epsilon}=1 \times 10^2$ s⁻¹ and $\dot{\epsilon}=5 \times 10^2$ s⁻¹ with the same loading rate $\dot{K}_I=1 \times 10^6$ MPa.m^{0.5}/s. It is clear from Figure 13(B) that the acceptable zone is slightly widened with the increasing strain rate, and the widened zone becomes larger with the increasing L_r .

Therefore, it should be noted that fracture assessment of the cracked structure made of ANSI 5140 steel must consider the effect of the loading rate, and the direct use of the quasi-static value may lead to dangerous results.

5 — CONCLUSIONS

The dynamic fracture behavior of AISI 5140 steel was studied over a wide range of loading rates. The following conclusions are drawn:

- (1) True stress-strain relations of AISI 5140 steel at different strain rates were measured, and a dynamic constitutive model was proposed. The steel is sensitive to strain rate and the flow stress increases with the increasing strain rate.
- (2) Fracture characteristics and fracture toughnesses of the steel were studied through the quasi-static test, instrumented Charpy impact test, and HPB impact test. Fracture toughness decreases with the increasing loading rate and fracture mechanisms are brittle fractures.
- (3) Based on the fracture assessment method of the CEGB R6 procedure, the effects of the strain rate and the loading rate are discussed. It is noted that the fracture assessment of the cracked ANSI 5140 steel structure must consider the effect of the loading rate, and the direct use of the quasi-static value may lead to dangerous results.

ACKNOWLEDGEMENTS

The authors gratefully acknowledge the support of National Natural Science Foundation of China (Grant No. 51305122) and National Basic Research Program of China (Grant No. 2012CB026003).

REFERENCES

1. Jones RL, Davies PC. Experimental characterization of dynamic tensile and fracture toughness properties. *Fatigue Fract Eng Mater Struct.* 1989; 12: 423-437.
2. Nam HS, Kim YJ, Kim JW, Kim JS. Energy-based numerical modeling of the strain rate effect on fracture toughness of SA508 Gr. Ia. *J Strain Anal Eng Des.* 2017; 52: 177-189.
3. Angamuthu K, Guha B, Achar DRG. Investigation of dynamic fracture toughness (J_{Id}) behaviour of strength mis-matched Q & T steel weldments using instrumented Charpy impact testing. *Eng Fract Mech.* 1999; 64: 417-432.

4. Sreenivasan PR, Mannan SL. Dynamic J-R curves and tension-impact properties of AISI 308 stainless steel weld. *Int J Fract.* 2000; 101: 229-249.
5. Jiang FC, Vecchio KS. Hopkinson bar loaded fracture experimental technique: a critical review of dynamic fracture toughness tests. *Appl Mech Rev.* 2009; 62: 060802.
6. Roudier PH, Francois D. Dynamic fracture toughness measurements and local approach modeling of titanium alloys. *Fatigue Fract Eng Mater Struct.* 1996; 19: 1317-1327.
7. Chaouadi R, Puzzolante JL. Loading rate effect on ductile crack resistance of steels using precracked charpy specimens. *Int J Pressure Vessels Pip.* 2008; 85: 752-761.
8. Foster JT, Chen W, Luk VK. Dynamic crack initiation toughness of 4340 steel at constant loading rates. *Eng Fract Mech.* 2011; 78: 1264-1276.
9. Prasad NE, Kamat SV, Malakondaiah G, Kutumbarao VV. Static and dynamic fracture toughness of an Al-Li 8090 alloy plate. *Fatigue Fract Eng Mater Struct.* 1994; 17: 441-450.
10. Wu QG, Chen XD, Fan ZC, Nie DF, Pan JH. Engineering fracture assessment of FV520B steel impeller subjected to dynamic loading. *Eng Fract Mech.* 2015; 146: 210-223.
11. Galvez F, Cendon D, Carcia N, Enfedaque A, Sanchez-Galvez V. Dynamic fracture toughness of a high strength armor steel. *Eng Fail Anal.* 2009; 16: 2567-2575.
12. Loya JA, Saez JF. Three-dimensional effects on the dynamic fracture determination of Al 7075-T651 using TPB specimens. *Int J Solids Struct.* 2008; 45: 2203-2219.
13. Cui XZ, Fan YF, Chen J. Experimental research of quasi-static and dynamic fracture toughness of 685 homogeneous steel. *Journal of Experimental Mechanics* 2012; 27: 326-334.
14. Wu QG, Chen XD, Fan ZC, Nie DF. Experimental and numerical study on dynamic fracture behavior of AISI 1045 steel for compressor crankshaft. *Fatigue Fract Eng Mater Struct.* 2017; 40: 245-253.
15. Lorentzon M, Eriksson K. Influence of intermediate loading rates and temperature on the fracture toughness of ordinary carbon-manganese structural steels. *Fatigue Fract Eng Mater Struct.* 1998; 21: 805-817.
16. Xu ZJ, Li YL. Dynamic fracture toughness of high strength metals under impact loading: increase or decrease. *Acta Mech Sin.* 2011; 27: 559-566.
17. Li YL, Guo WG, Jia DX, Liu YY, Luo JR, Du J, Chen YZ. Experimental measurement of dynamic fracture initiation toughness of 40Cr steel. *Explosion and Shock Waves.* 1996; 16: 21-30.
18. GB/T 21143-2007. *Metallic Materials-Unified Method of Test for Determination of Quasistatic Fracture Toughness.* Standards Press of China, Beijing.
19. GB/T 229-2007. *Metallic Materials-Charpy Pendulum Impact Test Method.* Standards Press of China, Beijing.
20. Magudeeswaran G, Balasubramanian V. Dynamic fracture toughness behavior of armor-grade Q & T steel weldments: effect of weld metal composition and microstructure. *Met Mater Int.* 2009; 15: 1017-1026.
21. Zehnder AT. *Fracture Mechanics. Lecture Notes in Applied and Computational Mechanics* 2012, Vol. 62, Springer, Netherlands.
22. R6. *Assessment of the integrity of structures containing defects, procedure R6-revision 4.* Gloucester: Nuclear Electric Ltd; 2001.

FIGURE CAPTIONS

FIGURE 1 Microstructure of the AISI 5140 steel

FIGURE 2 Experimental true stress-strain curves of the AISI 5140 steel

FIGURE 3 Yield strength of the AISI 5140 steel at different strain rates

FIGURE 4 Load-deflection curves of quasi-static specimens

FIGURE 5 Load-deflection curves of Charpy impact specimens

FIGURE 6 The experimental incident and reflected strain waves

FIGURE 7 Crack initiation signals of the test specimens

FIGURE 8 Displacement of the incident bar end initially in contact with the specimen

FIGURE 9 Finite element model of the incident bar, the specimen and the support

FIGURE 10 Numerical J -integral history at the crack tip

FIGURE 11 Fracture appearances of AISI 5140 steel. (A) quasi-static test, (B) instrumented Charpy impact test, (C) HPB impact test

FIGURE 12 Fracture toughnesses of the AISI 5140 steel under different loading rates

FIGURE 13 Failure assessment diagram of the AISI 5140 steel. (A) effect of loading rate, (B) effect of strain rate

NOMENCLATURE NOMENCLATURE

a_0	initial crack length
A_1, A_2, n	material constants related to strain hardening
B	thickness of specimen
c	sound speed in incident bar
c_1	experimental constant
C, p	material constant related to strain-rate hardening
D	displacement of incident bar end initially in contact with specimen
E	elastic modulus
F_Q	load at intersection point of load-deflection curve and line OF_d
J	J -integral
J_{Id}	dynamic fracture toughness
K_1	experimental constant
K_I	stress intensity factor
K_{IC}	static fracture toughness
K_{Id}	dynamic fracture toughness
\dot{K}_{Id}	loading rate
K_{Id}^r	reference fracture toughness value
\dot{K}_{Id}	reference loading rate
K_{rd}	ratio of stress intensity factor at crack tip to dynamic fracture toughness of material
L_{rd}	ratio of loading condition assessed for plastic limit load of structure $L_{rd} = \frac{\sigma_{ref}}{\sigma_{yd}}$
L_{rd}^{max}	cut-off value of L_{rd}
L	length of specimen
P_{max}	peak load
S	span of specimen
t_d	propagating time of strain wave from crack tip to position of strain gauge
t_f	crack initiation time
t_p	time corresponding to peak strain signal
W	width of specimen
ε_{eq}	equivalent strain

NOMENCLATURE **NOMENCLATURE**

$\dot{\epsilon}_{eq}$	equivalent strain rate
ϵ_i	incident strain
ϵ_r	reflected strain
σ_{eq}	equivalent stress
σ_{ref}	reference stress
ρ	density of incident bar
ν	Poisson's ratio

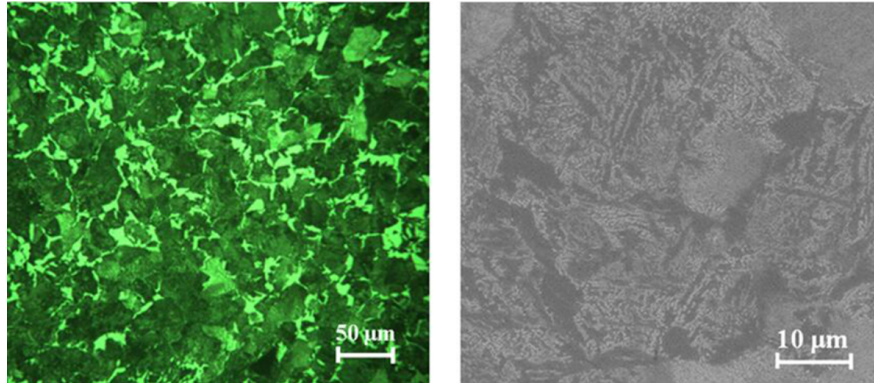


FIGURE 1 Microstructure of the AISI 5140 steel

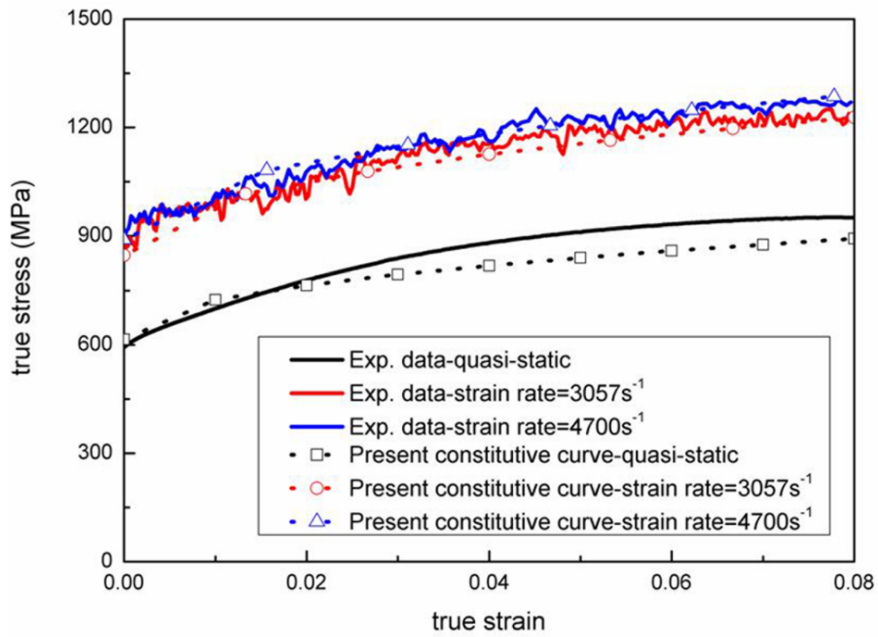


FIGURE 2 Experimental true stress-strain curves of the AISI 5140 steel

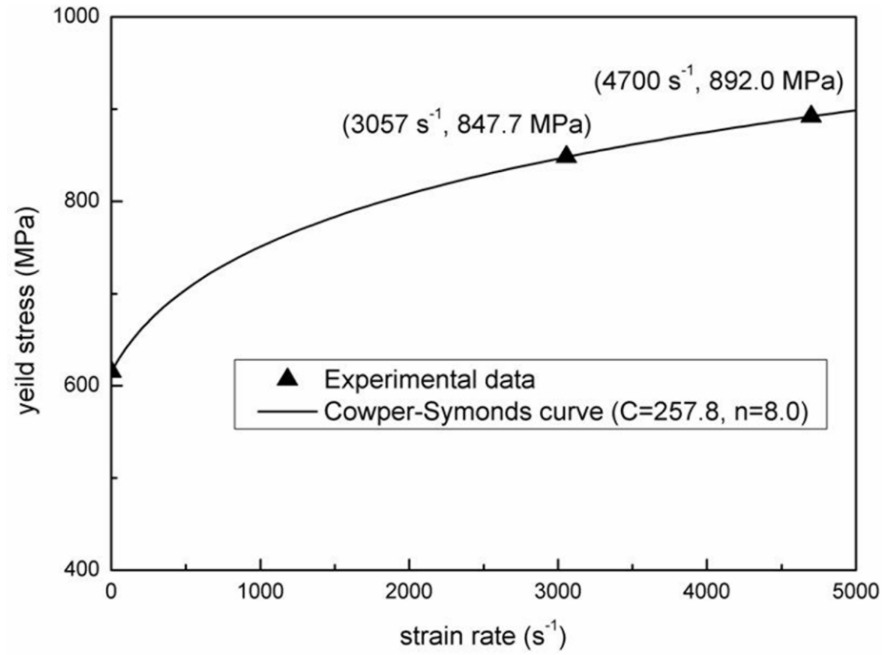


FIGURE 3 Yield strength of the AISI 5140 steel at different strain rates

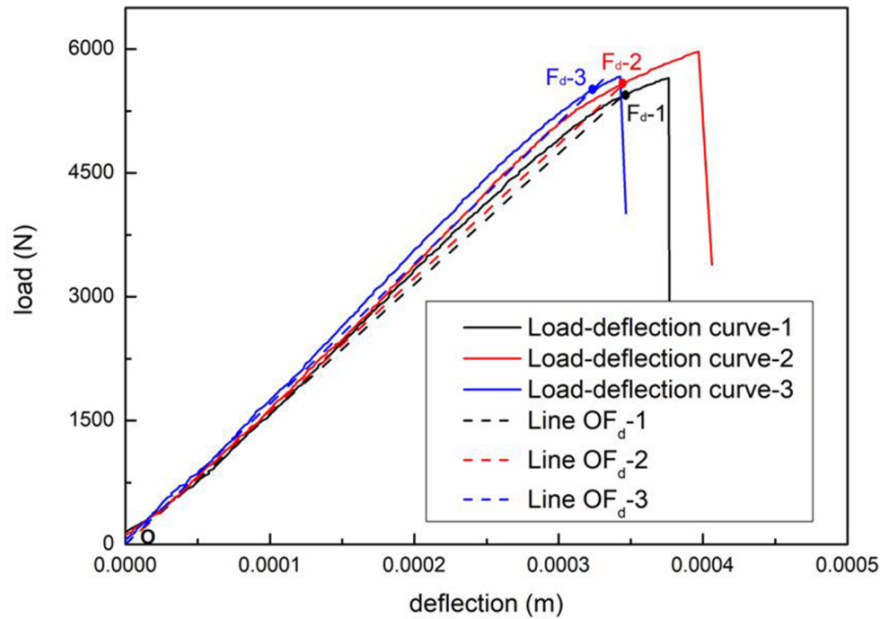


FIGURE 4 Load-deflection curves of quasi-static specimens

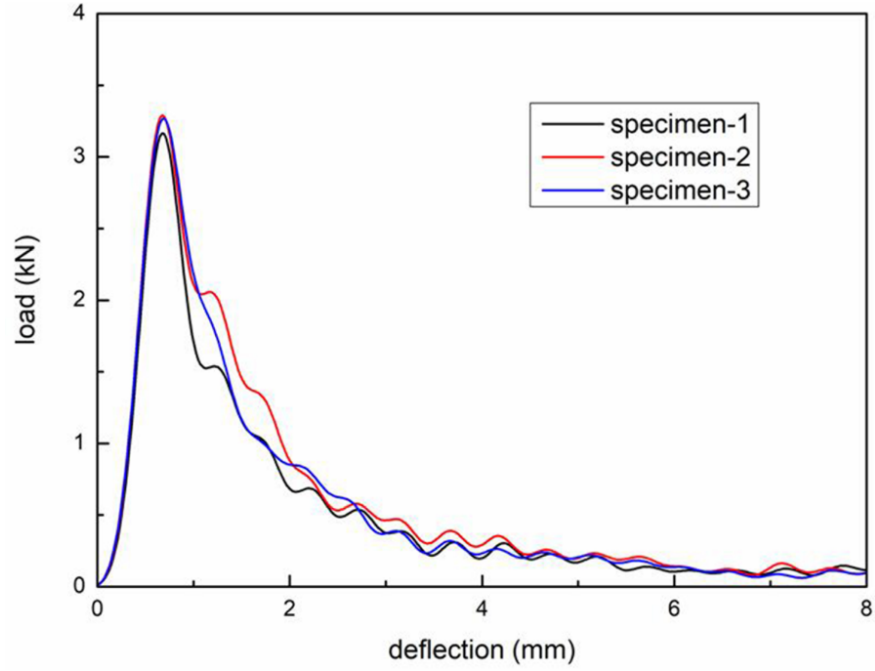


FIGURE 5 Load-deflection curves of Charpy impact specimens

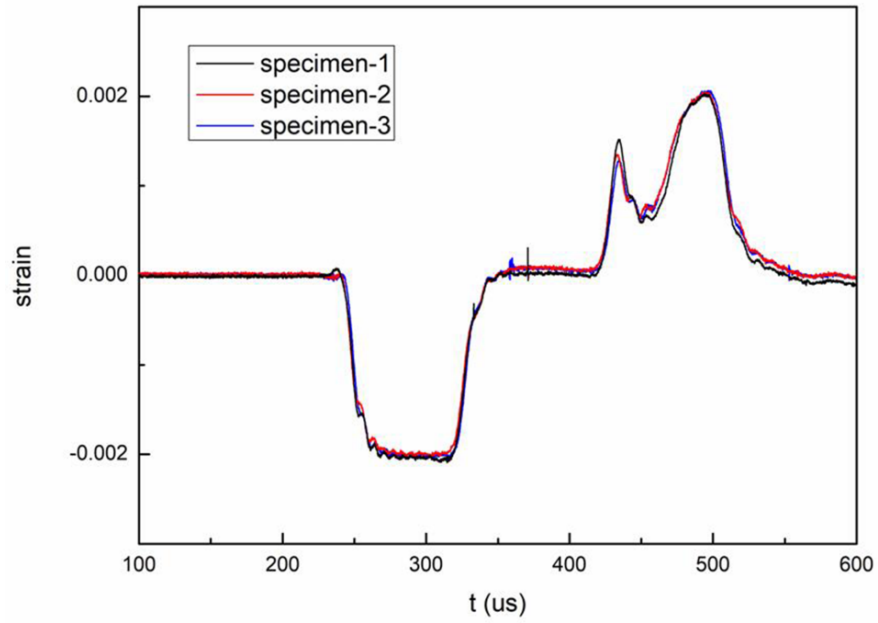


FIGURE 6 The experimental incident and reflected strain waves

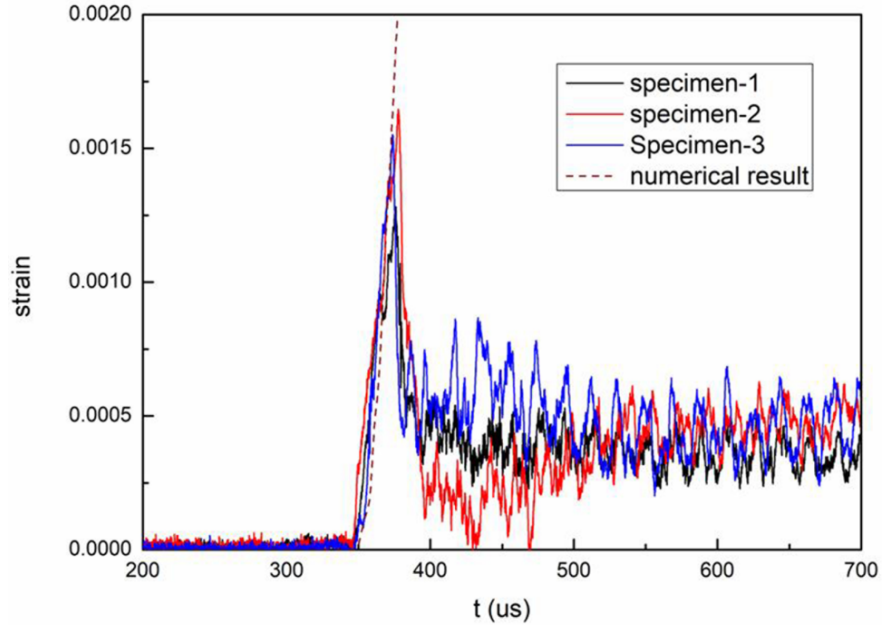


FIGURE 7 Crack initiation signals of the test specimens

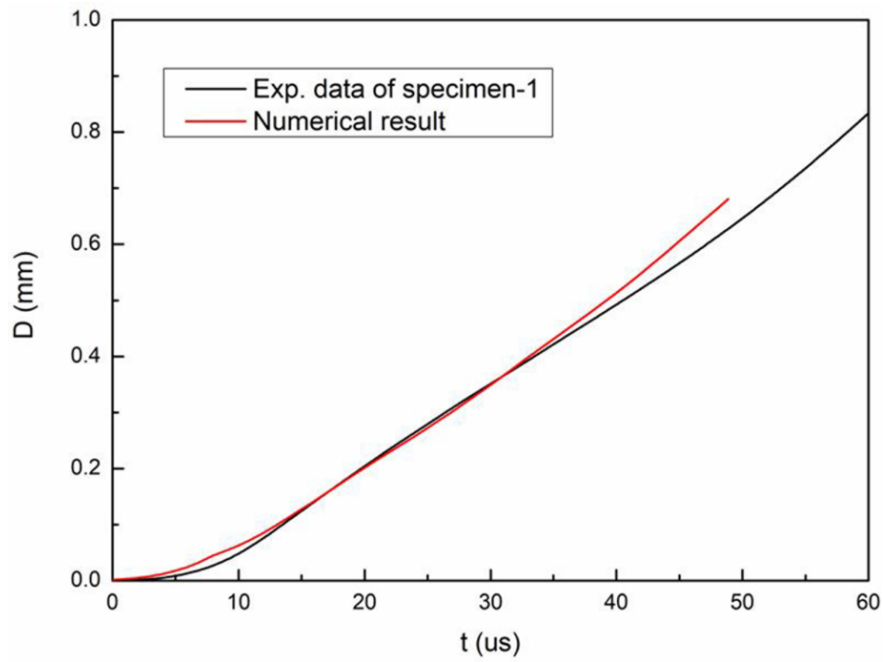


FIGURE 8 Displacement of the incident bar end initially in contact with the specimen

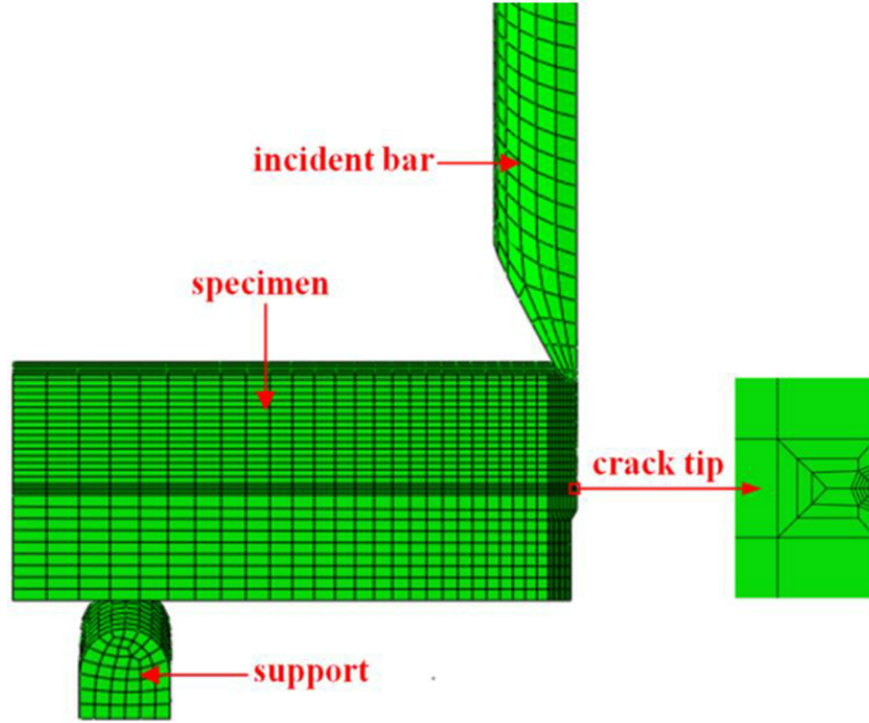


FIGURE 9 Finite element model of the incident bar, the specimen and the support

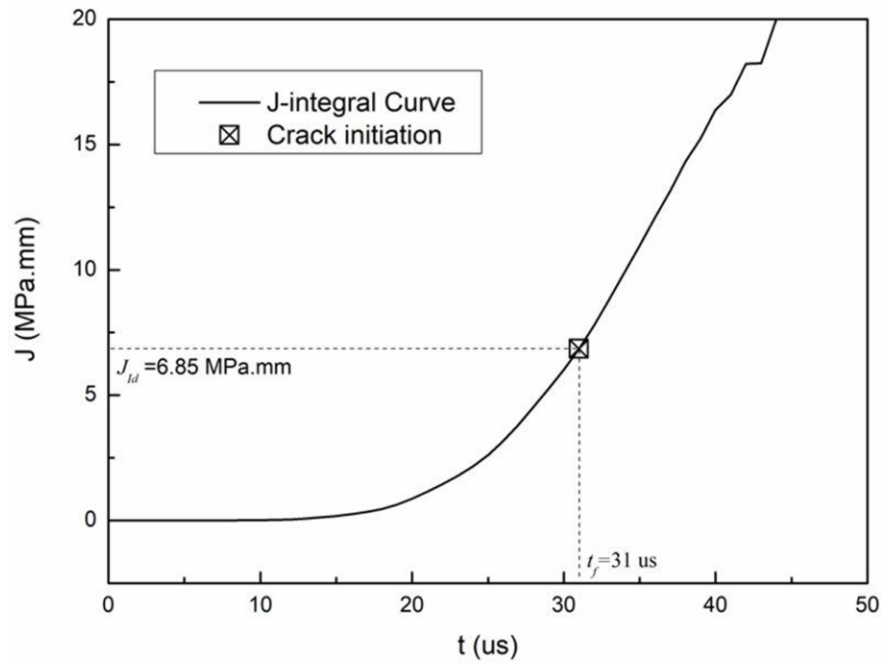


FIGURE 10 Numerical J -integral history at the crack tip

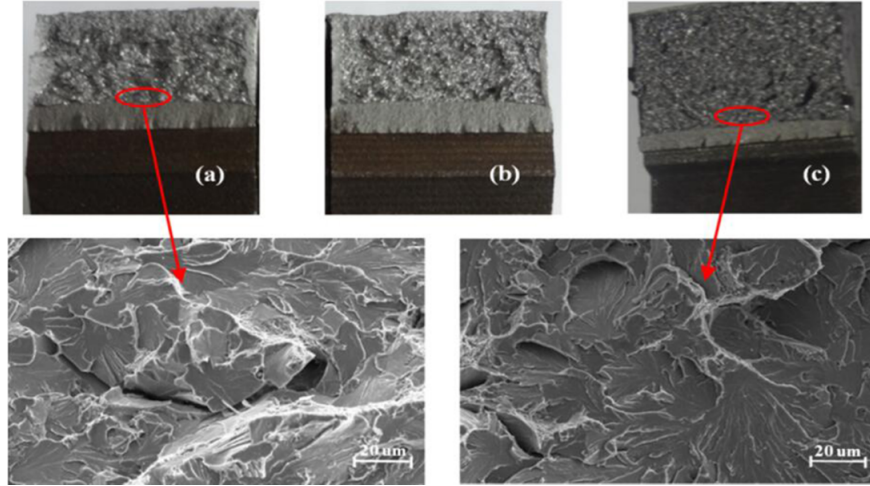


FIGURE 11 Fracture appearances of the AISI 5140 steel. (A) quasi-static test, (B) instrumented Charpy impact test, (C) HPB impact test

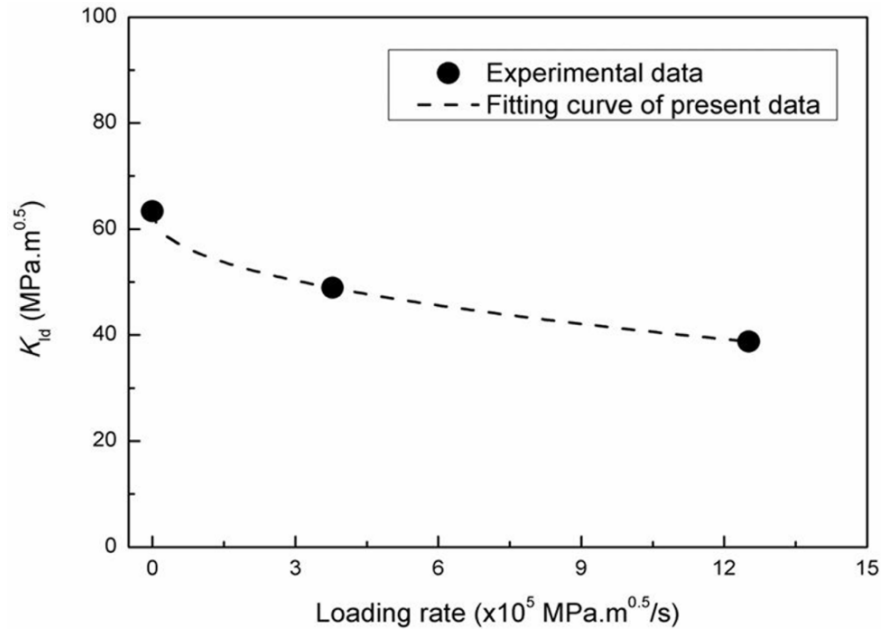
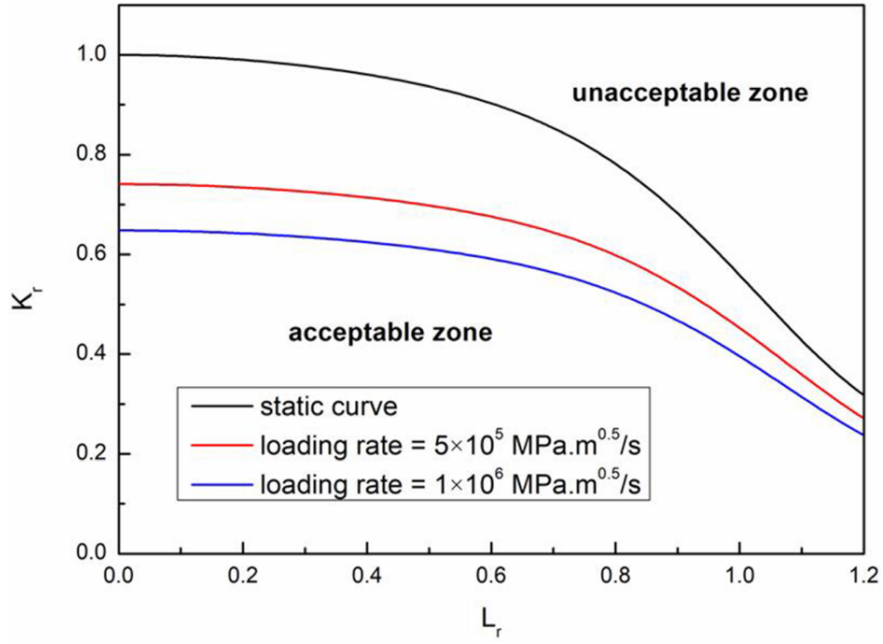
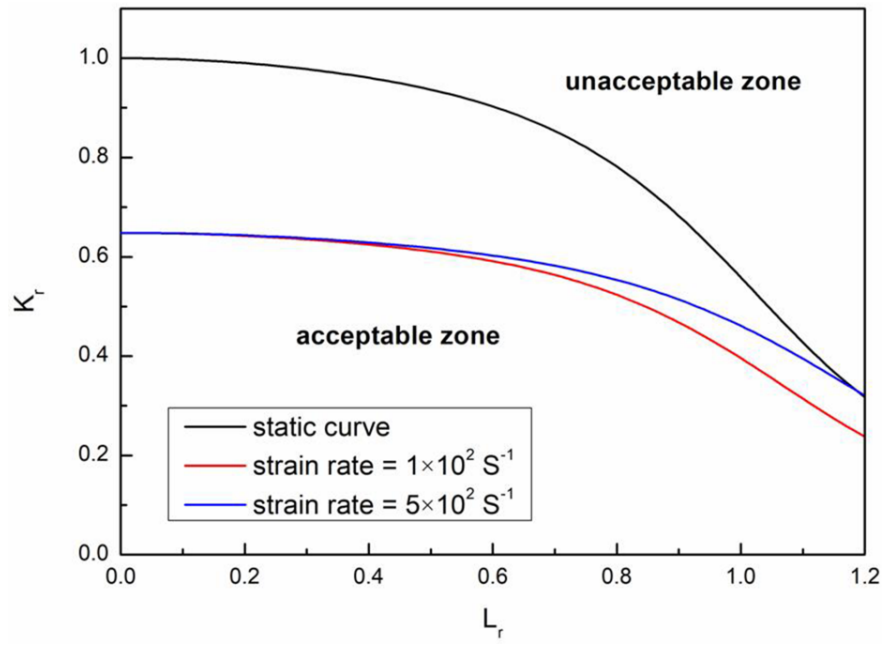


FIGURE 12 Fracture toughnesses of the AISI 5140 steel under different loading rates



(A)



(B)

FIGURE 13 Failure assessment diagram of the AISI 5140 steel. (A) effect of loading rate, (B) effect of strain rate

TABLE 1 Chemical compositions of the AISI 5140 steel (wt. %)

	C	Si	Mn	P	S	Cr	Ni	Cu
ASTM A29/A29M	0.38-0.43	0.15-0.35	0.70-0.90	[?]0.035	[?]0.040	0.70~0.90	[?]0.25	[?]0.35
Measured	0.44	0.25	0.59	0.021	0.007	0.85	0.04	0.05